www.elsevier.com/locate/memsci

Total water production capacity inversion phenomenon in multi-stage direct contact membrane distillation: A theoretical study

Jung-Gil Lee, Ahmad S. Alsaadi, Ayman M. Karam, Lijo Francis, Sofiane Soukane, Noreddine Ghaffour

PII: S0376-7388(17)32246-9
DOI: http://dx.doi.org/10.1016/j.memsci.2017.09.020
Reference: MEMSCI15558

To appear in: *Journal of Membrane Science*

Received date: 4 August 2017
Revised date: 4 September 2017
Accepted date: 5 September 2017

Cite this article as: Jung-Gil Lee, Ahmad S. Alsaadi, Ayman M. Karam, Lijo Francis, Sofiane Soukane and Noreddine Ghaffour, Total water production capacity inversion phenomenon in multi-stage direct contact membrane distillation: A theoretical study, *Journal of Membrane Science,* http://dx.doi.org/10.1016/j.memsci.2017.09.020

Total water production capacity inversion phenomenon in multi-stage direct contact membrane distillation: A theoretical study

Jung-Gil Lee[a], Ahmad S. Alsaadi[a], Ayman M. Karam[b], Lijo Francis[a], Sofiane Soukane[c], Noreddine Ghaffour[a,*]

[a]*King Abdullah University of Science and Technology (KAUST), Water Desalination and Reuse Center (WDRC), Biological & Environmental Science & Engineering Division (BESE), Thuwal 23955-6900, Saudi Arabia*

[b]*King Abdullah University of Science and Technology (KAUST), Computer, Electrical and Mathematical Science and Engineering Division (CEMSE), Thuwal 23955-6900, Saudi Arabia*

[c]*Institute of Marine Science and Coastal Management, Campus Universitaire de Dely Ibrahim, Bois des Cars, BP 19, 16320, Algiers, Algeria*

[*]*Corresponding author. Tel.: +966-128082180, E-mail address: noreddine.ghaffour@kaust.edu.sa*

Abstract

The low thermal efficiency and low water production are among the major challenges that prevent membrane distillation (MD) process from being commercialized. In an effort to design an efficient multi-stage direct contact MD (DCMD) unit through mathematical simulation, a new phenomenon that we refer to as total water production capacity inversion (WPI) has been detected. It is represented by a decrease in the total water production beyond a number of stages or a certain module length. WPI phenomenon, which was confirmed by using two different mathematical models validated experimentally, was found to take place due to the decrease in water vapor flux across the membrane as well as the increase in heat loss by conduction as the membrane length increases. Therefore, WPI should be considered as a critical MD design-criterion, especially for large scale units. Investigations conducted for a simulated multi-stage DCMD process showed that inlet feed and permeate temperatures difference, feed and permeate flow rates, and feed salinity have different effects on WPI. The number of stages (or module length at constant width) that leads to a maximum water production has been determined for different operating parameters. Decreasing inlet feed and permeate temperatures difference, or inlet feed and permeate flow rates and increasing inlet feed temperature at constant temperature difference or inlet feed salinity cause the WPI to take place at lower number of stages. Even though the feed salinity affects negligibly the

mean permeate flux, it was clearly shown that it can affect WPI. The results presented herein unveil a hidden phenomenon that is likely to occur during process scale-up procedures and should be considered by process engineers for a proper choice of system design and operating conditions.

Keyword: Thermal equilibrium; DCMD module scale-up; Total water production; Total heat flux; Conduction heat loss.

1. Introduction

Membrane distillation (MD) is a thermal separation process that utilizes a hydrophobic micro-porous membrane to achieve separation by partial pressure difference (created by temperature difference) between two hydrophilic fluids [1]. The MD process has several advantages [1-23], such as: (i) low sensitivity towards feed water salinity compared to other matured desalination technologies such as reverse osmosis (RO) [2, 8, 22, 23] , (ii) near 99.99% rejection of non-volatile electrolytes which include sodium chloride (NaCl), potassium chloride (KCl) and lithium bromide (LiBr) as well as non-electrolytes such as glucose, sucrose and fructose in aqueous solutions [7, 20], (iii) relatively low requirement of operating temperature and hydraulic pressure compared to thermal or membrane based processes (e.g., multi-stage flash or RO)[6, 20], respectively, (iv) small foot print [21], and (v) potentially low maintenance cost. Therefore, many researchers have studied MD as a potential process for seawater desalination. Even though it can be built at lower capital cost, the main drawback of the MD process is its high-energy requirement, which is a characteristic of all thermally driven processes [6]. Many studies [24-26] have been conducted to enhance the MD system performance such as the use of heat recovery concept, the utilization of sustainable energy sources such as geo- or solar-thermal energy to reduce water production cost [8, 27, 28].

MD has four major process configurations, namely direct contact MD (DCMD), air gap MD (AGMD), sweeping gas MD (SGMD) and vacuum MD (VMD). Other configurations based on the conventional ones, such as liquid/water gap MD or material gap MD, are also possible [15]. Among them, DCMD has the simplest configuration and can produce higher permeate flux [20]. However, this module configuration suffers from the highest heat loss through conduction across the membrane compared to the other configurations.

Several studies focused on MD process scale-up and its viability at the industrial level mainly using multi-stage or multi-effect concepts [2-4, 8, 29-34]. It has been shown that increasing membrane surface area (module length) is necessary to increase MD thermal efficiency at constant flow-rate [16] which clearly encourages the use of multiple stages concept. Within this scope, Lee et al., [2] developed a hybrid multi-stage VMD and pressure retarded osmosis (PRO) with recycling scheme to investigate the synergy of the hybrid system. The multi-stage concept is employed to increase the water production. The recycling scheme is applied to the multi-stage VMD system for the continuous production of highly concentrated brine. The concentrated brine produced from the multi-stage VMD with recycling system is then supplied as a draw solution to the PRO system for power generation. Lee and Kim [3] and González-Bravo et al., [29] have investigated the scenarios of a multi-stage MD process with different configurations such as series, parallel and series/parallel arrangement of MD modules to find the optimal design of the multi-stage concept. Kim et al., [8, 32] and Lee et al. [23] reported the solar-assisted multi-stage VMD and DCMD systems with heat recovery unit and their effect on water production and specific thermal energy consumption with systems reaching 30 stages aiming to enhance the internal heat recovery. In thermally-driven processes, such as multi-stage flash (MSF), the high thermal efficiency is achieved through multiple stages (e.g. 24 very large stages are typically used in MSF plants) in order to run the evaporation/condensation cycle in each stage at very low temperature difference (2-5 ^{o}C). Similar concept is required to scale-up the MD process efficiently.

All these studies have reported that the total water production capacity increases while the mean permeate flux decreases when the module length is increased (at constant membrane width). The effect of membrane area on water production, thermal efficiency and mean permeate flux was attributed to the higher residence time when longer channel is used. Indeed, increasing channel length leads to a significant reduction of the feed and permeate temperature difference and thus a decrease in the driving force across the membrane. However, to the best of our knowledge no research has been reported on the possibility of total water production inversion (WPI) in DCMD process when a large number of modules/stages or equivalently a long single MD module is used.

WPI has been noticed during scale-up design procedures using mathematical modeling. Simulation of large scale multi-stage MD module using a previously reported mathematical model validated experimentally [1] seemed to exhibit WPI beyond a given module length.

This observation has been further investigated and results confirmed this distinctive behavior for thermal efficiency using another mathematical model based on a lumped-parameter dynamic predictive approach which was validated experimentally [35, 36]. At constant inlet conditions of feed and permeate and different membrane surface area (module length at constant width), DCMD mathematical modeling showed that total water production increases as the module length increases then decreases after the maximum water production value is reached. Therefore, in this paper we attempt to bring explanations to this observed phenomenon. Furthermore, the effect of key operational parameters on the maximum water production value from which WPI occurs inside the multi-stage DCMD system are discussed. These include inlet feed salinity, and inlet feed and permeate temperatures difference, as well as inlet flow rates.

2. Theoretical approach

2.1 Mathematical models

In this study, two previously reported DCMD mathematical models with different solution algorithm were used [1, 35, 36]. The first steady-state mathematical model (model A) is discretized on one-dimensional grid and its source code is developed in-house. The set of ordinary differential equations that govern the heat and mass transfer inside the DCMD system were solved simultaneously using Broyden's method. All thermophysical properties of seawater used in this mathematical model were obtained from Sharqawy et al. [37]. The second mathematical model (model B) takes into account the dynamics of the process and is based on the lumped-capacitance method, where the module is divided into small control-volume cells where heat and mass conservation equations are developed. Then, the overall model is derived by coupling neighboring cells together using the analogy between thermal and electrical systems. The resultant model is a system of nonlinear differential algebraic equations, which accounts for the spatial and temporal temperature distribution inside the DCMD module. It is implemented in MATLAB environment and allows the user to easily set-up the model to simulate various operating conditions and predict the transient and steady-state DCMD process operation. Additionally, it can predict scaled-up systems thus facilitating module design, and process optimization [35, 36].

Both model [A] and model [B] assumed the negligible conduction and convection heat transfer to the surrounding atmosphere. The main difference between the two models is that model [A] couples momentum, heat and mass transfer in a steady state one-dimensional formulation, while model [B] considers only heat and mass transfer transient balance along the module. In addition, both of simulation results showed a maximum 10% of deviation with experimental data [1, 36]. However, both mathematical models were validated against experimental data (for detailed explanation of theoretical background, equations used and solution procedures, please refer to [1, 35, 36]).

2.2 Simulated DCMD setup

These mathematical models were used to simulate multiple cascaded stacks of flat-sheet DCMD membrane modules arranged in series with a heat recovery system (**Fig. 1**). The DCMD set up consists of two main streams, namely the permeate stream (blue line) and seawater stream (red line). A heat exchanger (HX) is set to heat up the incoming seawater by recovering the heat from the exiting permeate flow. The inlet feed seawater concentration is kept constant by controlling the quantity of discharge brine. The inlet feed and permeate temperatures were kept constant by using the external heater and the air cooler, as shown in Figure 1. Each stage in this configuration has a dimension of 0.5 m width and 0.6 m length. The feed and permeate flow in a counter current flow mode through all stages inside a channel height of 0.003 m. A commercial composite membrane was used in this study, which consists of a polytetrafluoroethylene (PTFE) active layer and poly-propylene (PP) scrim-backing support layer. Properties of the composite membrane are reported in Table 1 [1]. Polypropylene mesh spacer was used as a turbulent promoter on both sides of the composite membrane [1, 38-41]. The properties of the spacer are presented in Table 2 [1].

Table 1. Characteristics of the PTFE/PP composite membrane [1].

Material	PTFE (active layer)	PP (support layer)
Thickness[A], δ_m (μm)	20±2	80±2
Porosity[A], ε (%)	70±5	34±5
Mean pore size[A], r (μm)	0.5±0.02	0.1±0.02
Liquid entry pressure[B], LEP_w (kPa)	207	160

A: measured values

B: Data provided by the manufacturer

Table 2. Specifications of the spacer [1].

Material	PP
Spacer thickness, h_s (mm)	0.8
Filaments diameter, d_f (mm)	0.4
Angle between filaments, θ (deg)	90
Mesh size, l_m (mm)	2

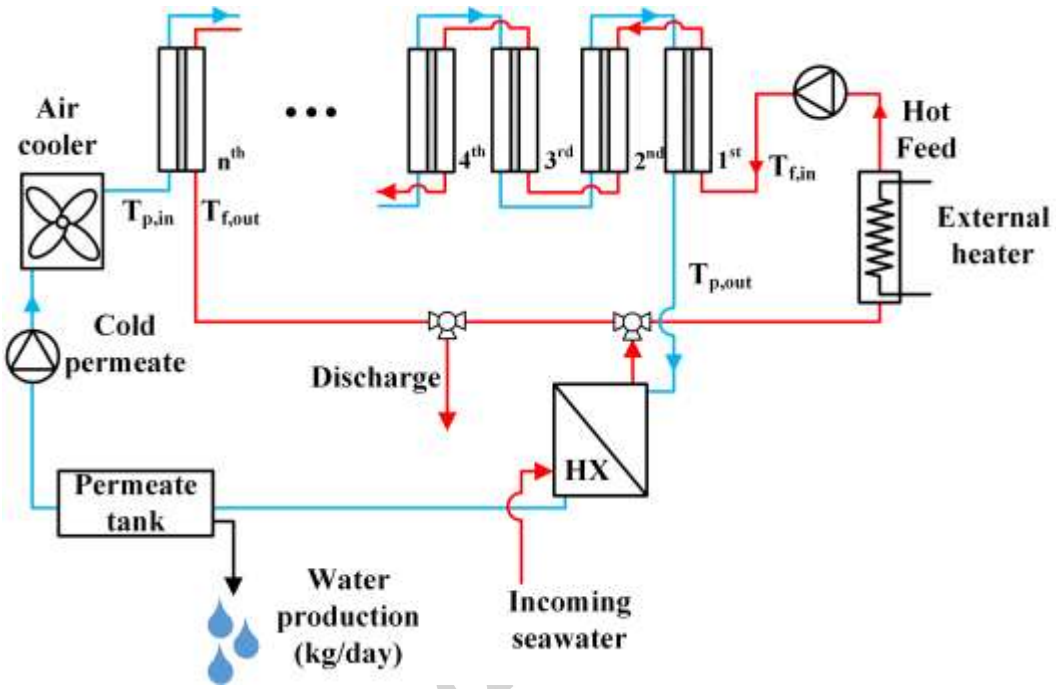

Figure 1. Simulated multistage DCMD setup.

2.3 Simulated DCMD scenarios

In order to assess the WPI phenomenon, several simulation cases were conducted which are summarized in Table 3:

Table 3. Simulated cases of multistage DCMD in this study.

Case	Objectives	Feed			Permeate	
		$\dot{m}$ (L/min)	T (°C)	S (g/kg)	$\dot{m}$ (L/min)	T (°C)
1	Difference between DCMD module and heat-exchanger	10	70	40	10	50
2	Effect of inlet feed and permeate temperatures difference	10	70	40	10	30 40 50
3	Effect of inlet feed	10	40	40	10	20

	temperature at constant temperature difference		50 60 70 80			30 40 50 60
4	Effect of inlet flow rate	10 15 20 25	70	40	10 15 20 25	30
5	Effect of inlet salinity	10	70	40 50 60 70 80	10	30

3. Results and discussion

3.1 Model comparison for water production inversion phenomenon

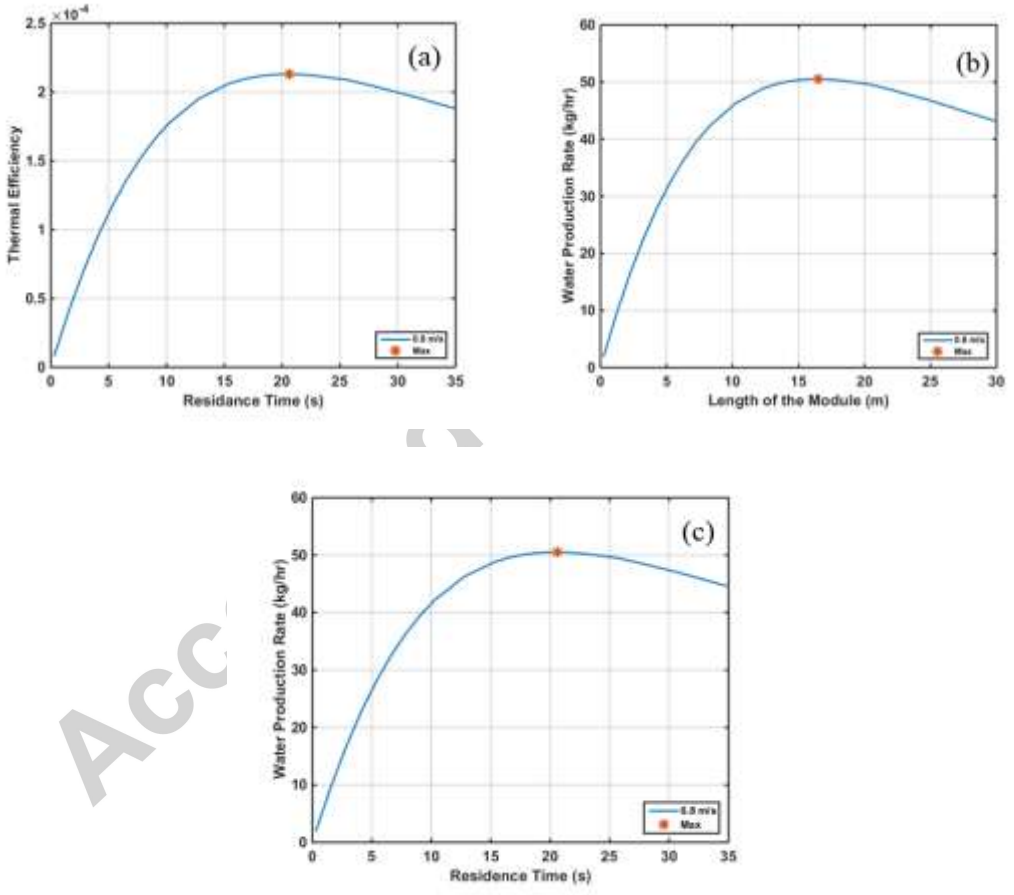

Residence time (Res_{time} = *module length/inlet feed velocity*)

Figure 2. (a) Thermal efficiency versus residence time [36], and total water production showing WPI phenomenon versus (b) module length and (c) residence time as predicted by model B. The maximum water production values are marked with a star on the curves.

Thermal efficiency and total water production capacity simulation results obtained with model B are presented in **Fig. 2**. Karam et al., [36] calculated the thermal efficiency (*T.E*) using the following equation:

$$T.E = J_m A \Delta H_v / \dot{m}_{f,in} c_p T_{f,in} \quad (1)$$

where J_m is the mean water vapor flux, A is the effective area, $J_m A$ is the water production ratio, and ΔH_v is the enthalpy of vaporization.

Eq. (1) is the ratio of the latent heat of water vapor evaporation transferred by mass transfer to the total heat introduced in the feed channel. It is clearly shown from Figure 2 that model [B] exhibits the WPI phenomenon with a decrease of thermal efficiency as residence time increases (Figure 2a) as well as a decrease in water production capacity when a given membrane length/number of modules (Figure 2b) or residence time (Figure 2c) is reached (additional data can be found in [36]). Details on the reasons behind this phenomenon are discussed in the next sections using simulation data obtained with model [A].

3.2 Comparison between DCMD module and heat exchanger device

For an in-depth understanding of the WPI phenomenon it is worth investigating the difference between a DCMD module and a classical heat-exchanger device. Therefore, the membrane permeability is set to zero and simulations are carried out in a so called zero DCMD mass flux (zDCMD) mode. In this mode, no heat transfer takes place by water vapor mass transfer and the only heat exchange between the feed and permeate sides occurs by conduction. In the first case (see case 1 in Table 3), experiments with feed and permeate inlet temperatures of 70 °C and 50 °C, respectively, feed and permeate inlet flow rates of 10 L/min, and feed solution salinity of 40 g/L (typical Red Sea water), were conducted. As shown in **Fig. 3**, one of the major differences between DCMD and zDCMD modes is the behavior of the total heat exchanged between fluids at different surface exchange areas. The total heat exchanged in zDCMD mode approaches a maximum with a plateau as the surface area increases while the total heat exchanged in the DCMD mode reaches a maximum value for a given module length and then starts to decrease. Such a behavior suggests that the WPI phenomenon is attributed to the contribution of water vapor mass transfer in the DCMD mode. To illustrate this relation lets discuss the total heat exchanged in both DCMD and zDCMD modes. The heat that can be exchanged by zDCMD mode can be described by the

following equation:

$$THX_{zDCMD} = \dot{m}_{f,in} c_{p,f} \Delta T_f = \sum_{i=1}^{n} \frac{kA_i}{\delta_m} (T_{f,m}^{(i)} - T_{p,m}^{i}) \quad (2)$$

where ΔT_f is the feed temperature difference between inlet and outlet, $T_{f,m}$ and $T_{p,m}$ are the inlet feed and permeate transmembrane temperatures, respectively, k is the conductivity of the membrane, δ_m is the membrane thickness,

However, the heat exchanged by DCMD module depends on both the water vapor flux and heat conduction and it can be expressed as:

$$THX_{DCMD} = \dot{m}_{f,in} c_{p,f} T_{f,in} - (\dot{m}_{f,in} - (J_m A)) c_{p,f} T_{f,out} = \sum_{i=1}^{n} J^{(i)} A_i \Delta H_v^{(i)} + \sum_{i=1}^{n} \frac{kA_i}{\delta_m} (T_{f,m}^{(i)} - T_{p,m}^{i}) \quad (3)$$

where $T_{f,\text{out}}$ is the outlet feed temperature, and $(T_{f,m} - T_{p,m})_m$ is the mean transmembrane temperature difference, and n the number of elements generated in the 1D discretized model.

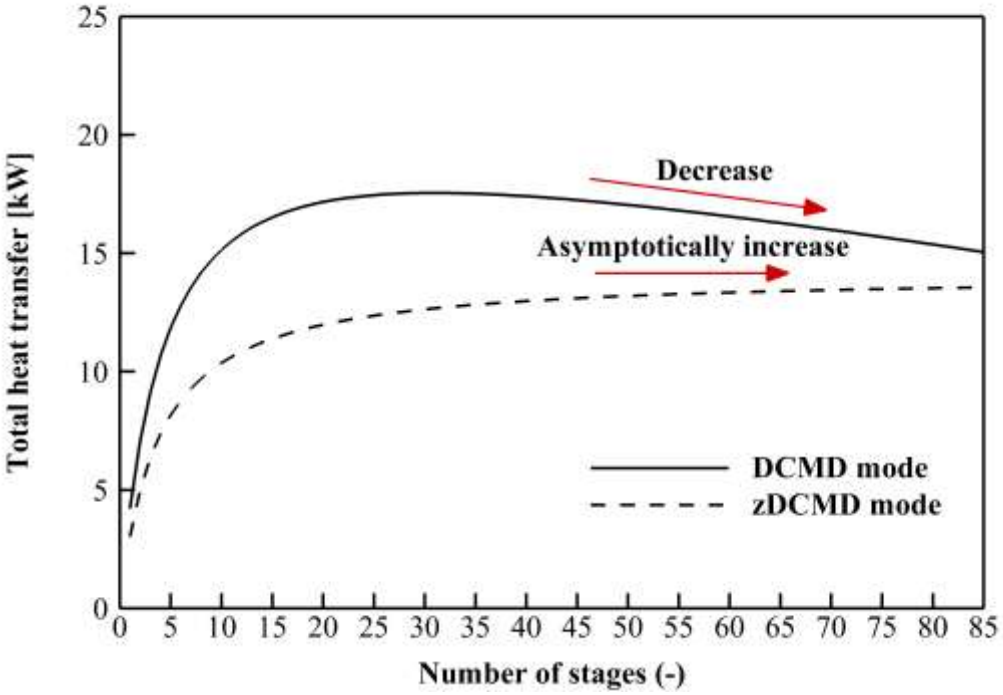

Figure 3. Comparison between the total heat transfer exchanged in DCMD and zDCMD modes as a function of number of stages at feed and permeate inlet temperatures of 70 °C and 50 °C, respectively, feed and permeate inlet flow rates of 10 L/min, and feed solution salinity of 40 g/L (typical Red Sea water) (case 1).

Simulations were carried out to investigate the effect of mass transfer on total heat transfer along the module length. **Fig. 3** shows that the transferred heat (latent heat by mass transfer + thermal conduction heat loss) increases to a maximum value (at 20th stage), and the maximum water production is achieved at that point (20th stage). This indicates that although conduction losses can affect total heat transfer, the highest heat transfer observed in DCMD mode is caused by mass transfer contribution, thus latent heat. The reduction in mass transfer (permeate flux) due to the increase in module length seen after the 20th stage affects significantly the total heat transfer. Mathematically, when $\dot{m}_{f,in} = J_m A$ (we refer to this extreme mathematical case as the complete mixing of the feed into the permeate stream) the maximum heat transfer is $\dot{m}_{f,in} c_p T_{f,in}$. At infinite membrane surface area, $J_m A$ is close to zero as the driving force (ΔT) tends to zero. In this case, the total heat exchanged in DCMD approaches that of the heat exchanger, as shown in **Fig. 3**. Between these two extreme values, there is a point where $J_m A$ in Eq. (3) reaches its maximum value, which is the point we referred to as WPI. In summary, the decrease of heat transfer after the 20th stage is mainly caused by the decrease of water production since mass transfer drops exponentially with feed transmembrane temperature thus leading to WPI.

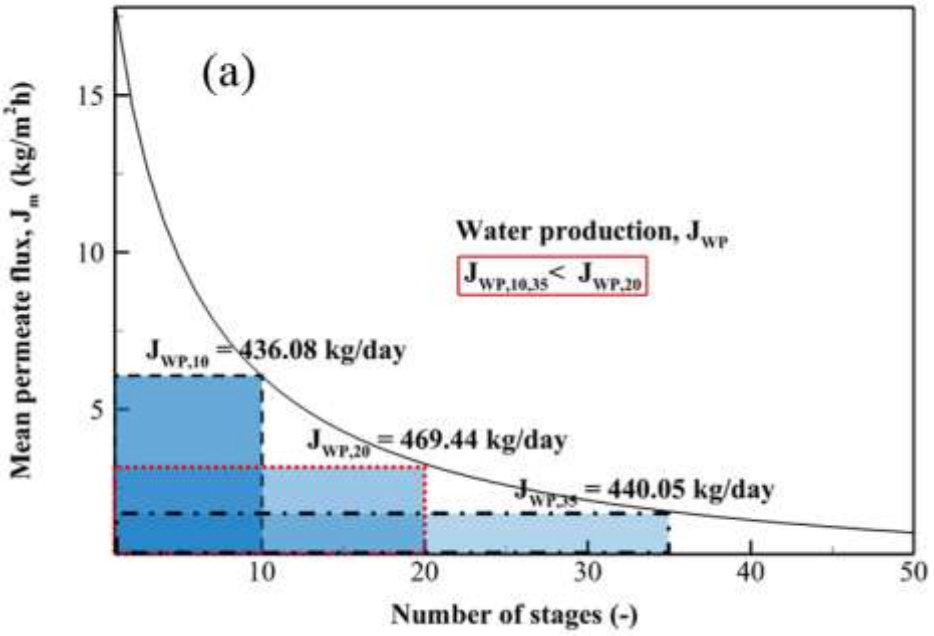

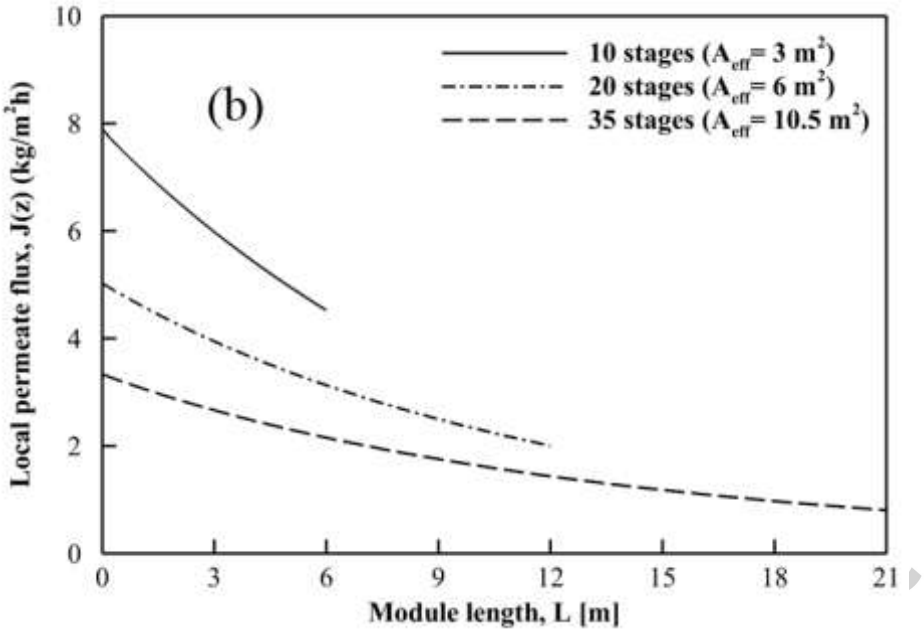

Figure 4. Effect of increasing module length at constant membrane width on (a) mean water vapor flux (J_m) and the total water production (J_{WP}) of multi-stage DCMD process, and (b) permeate flux (J(x)) along the module length at feed and permeate inlet temperatures of 70 °C and 50 °C, respectively, feed and permeate inlet flow rates of 10 L/min, and feed solution salinity of 40 g/L (typical Red Sea water) (case 1).

Beyond the observed maximum value, any increase in membrane surface area (increase of module length at constant membrane width) causes a decrease in the average flux by a greater magnitude than the gain resulting from an increase in the membrane surface area (**Fig. 4(a)**). This is because typically the transmembrane temperature difference and partial water vapor pressure difference decreases with an increase in the number of stages or module length (effective area) due to the decrease of the convection heat transfer coefficient and the increase of the conduction heat loss along the channel length [1]. The convection heat transfer coefficient decreases as the module length increases due to the decrease of the flow velocity resulting from the water vapor passing through the membrane however its effect remains negligible. The conduction heat loss also increases with an increase in the effective area. Furthermore, the feed salinity increase along the axial distance can lead to a decrease in the transmembrane temperature difference as driving force that resulted from the decrease of the specific heat capacity (see **Fig. S1** in the supplementary information). This means that the local permeate flux along the module length decreases as the module length increases and the

effect can be significant in case of longer module or high number of stage in series, as shown in **Fig. 4(b)**. Therefore, during the design of a DCMD module, the module length should not exceed this point from an operational point of view.

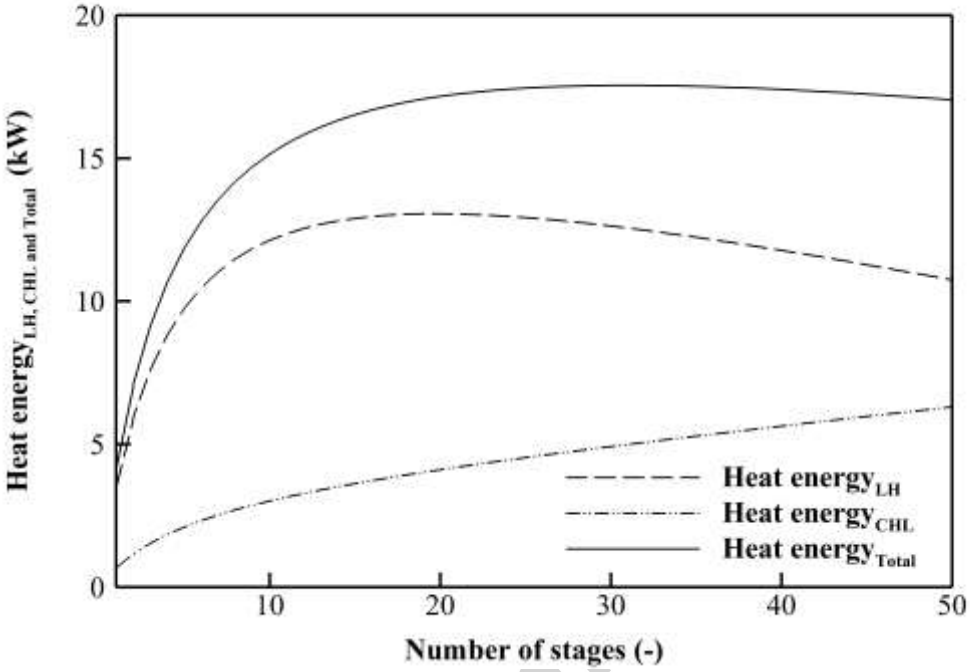

Figure 5. Average heat transfer contributions inside the DCMD module as a function of module length at feed and permeate inlet temperatures of 70 °C and 50 °C, respectively, feed and permeate inlet flow rates of 10 L/min, and feed solution salinity of 40 g/L (typical Red Sea water) (case 1). Heat transfer$_{LH}$ is the latent heat transfer, Heat transfer$_{CHL}$ is the conduction heat loss, and Heat transfer$_{Total}$ is the total heat transfer.

As shown in **Fig. 5**, the two types of heat transfer mechanisms such as latent heat transfers and conduction heat loss inside the DCMD module have different behaviors as the membrane length increases. The total heat exchanged in the DCMD system consists of the latent heat and the conduction heat loss. One is referred to the summation of the latent heat which is carried by water vapor mass as it passes through the membrane pores is represented by the following equation:

$$Heat\ transfer_{LH} = J_m A \Delta H_v \quad (4)$$

The second type is referred to as heat loss and transferred through conduction and is

represented mathematically by the following equation:

$$Heat\ transfer_{CHL} = \frac{kA}{\delta_m}(T_{f,m} - T_{p,m})_m \quad (5)$$

The latent heat energies increase with an increase in the number of stages up to 20 stages and then decreases, as shown in **Fig. 5**. This is because the conduction heat loss contribution in the total heat balance increases linearly with respect to the increase of effective area. And it also means that the partial vapor pressure of feed side decreases along the module length due to the decrease in the feed temperature resulting from the thermal energy consumption for the water vapor evaporation beyond 20 stages. The partial water vapor pressure is a function of the transmembrane temperature and salinity of solution as expressed in Eqs. ((6) and (7)).

$$P_{w,m} = \exp\left(23.1964 - \frac{3816.44}{T_m - 46.13}\right) \quad (6)$$

$$P_{f,m} = \left(1 - x_f\right) P_{w,m} \quad (7)$$

where $P_{w,m}$ and $P_{f,m}$ are the partial pure water vapor pressure and the partial saline water vapor pressure, respectively, T_m is the transmembrane temperature, and x_f is the molar fraction of non-volatile solute.

The conduction heat loss increases relatively at higher rate in the few first stages due to the higher transmembrane temperature differences near the feed inlet. However the conduction heat loss increases almost linearly at lower rate with the increase in number of stages. It means that the mean transmembrane temperature difference decreases with an increase in the number of stages. It will converge to small values which will generate few water vapor and the increase of effective area only can affect the increase of the conduction heat loss.

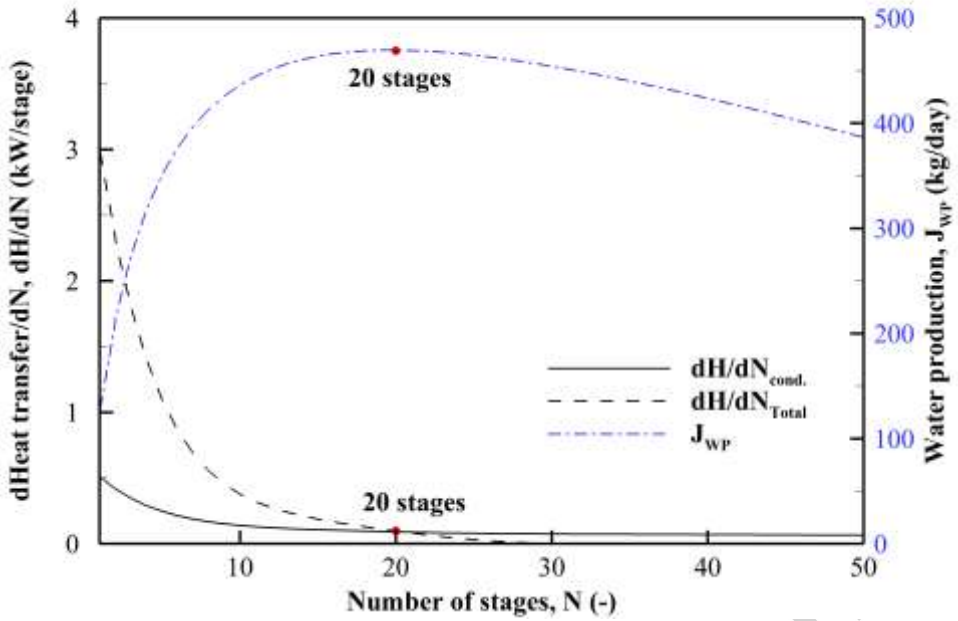

Figure 6. Rate of change of total heat and conductive heat transfer inside the DCMD module with respect to the change in MD membrane surface area and the corresponding total water production at feed and permeate inlet temperatures of 70 °C and 50 °C, respectively, feed and permeate inlet flow rates of 10 L/min, and feed solution salinity of 40 g/L (typical Red Sea water) (case 1).

To better assess the sensitivity of the total heat with respect to membrane surface area, a polynomial curve fitting is applied to the curves in **Fig. 5** followed by a differentiation of the polynomials with respect to membrane surface area. The resulting curves are represented in **Fig. 6**. It can be noticed that the derivative of total heat with respect to module length (or number of stages) intersects the derivative of the heat transfer by conduction at the WPI point where the derivative of the heat transfer by water vapor mass is close to zero (maximum point).

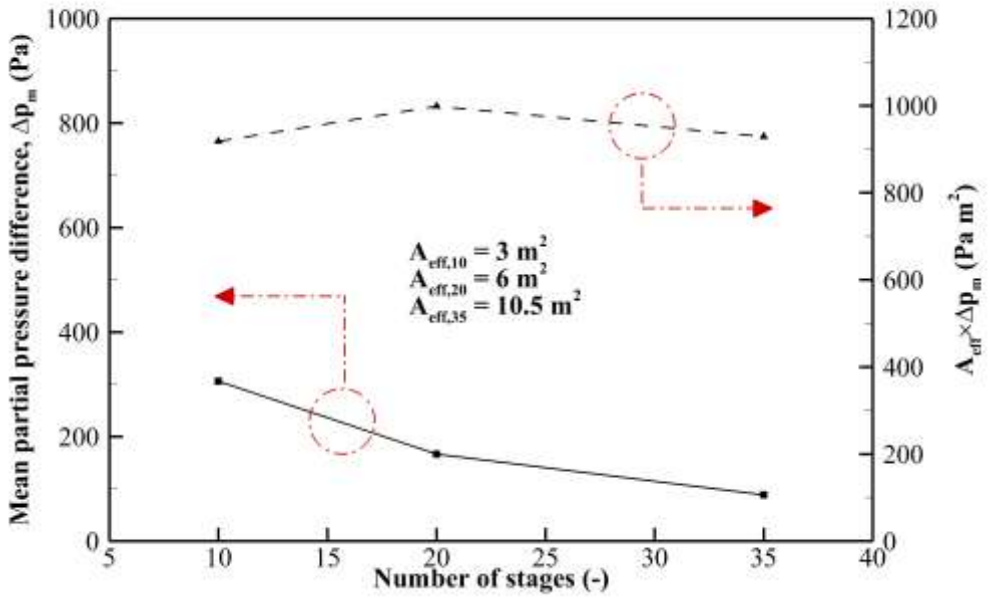

Figure 7. Mean partial pressure difference and the $A_{eff} \times \Delta p_m$ with respect to the number of stages at feed and permeate inlet temperatures of 70 °C and 50 °C, respectively, feed and permeate inlet flow rates of 10 L/min, and feed solution salinity of 40 g/L (typical Red Sea water) (case 1).

The mean partial pressure difference as driving force, Δpm and its product with the effective area, Aeff×Δpm were investigated for different number of stages, namely 10, 20 and 35 (see Fig. 7). In accordance with the WPI occurrence, the mean partial pressure difference decreases as the number of stage increases. However the Aeff×Δpm reaches the maximum value at 20 stages.

3.3 Influence of feed and permeate inlet temperatures difference

The effect of varying the feed and permeate inlet temperatures difference from 20 °C to 40 °C was examined by conducting the simulation case 2, presented in Table 3. As shown in Fig. 8, increasing the feed and permeate inlet temperatures difference caused the WPI to take place at higher membrane surface area (higher number of DCMD stages). Changing the inlet feed and permeate temperatures difference from 40°C to 20°C caused the WPI to occur at stage 20 instead of stage 33. The low inlet feed and permeate temperature difference can accelerate the WPI.

Water production decreases with feed and permeate inlet temperature difference as shown in Fig. 8. Moreover, WPI occurs at an earlier stage at lower feed and permeate inlet feed temperature difference. Therefore, the lower feed and permeate inlet feed temperature difference drives the convergence of the transmembrane temperature difference to its lowest value at an earlier stage.

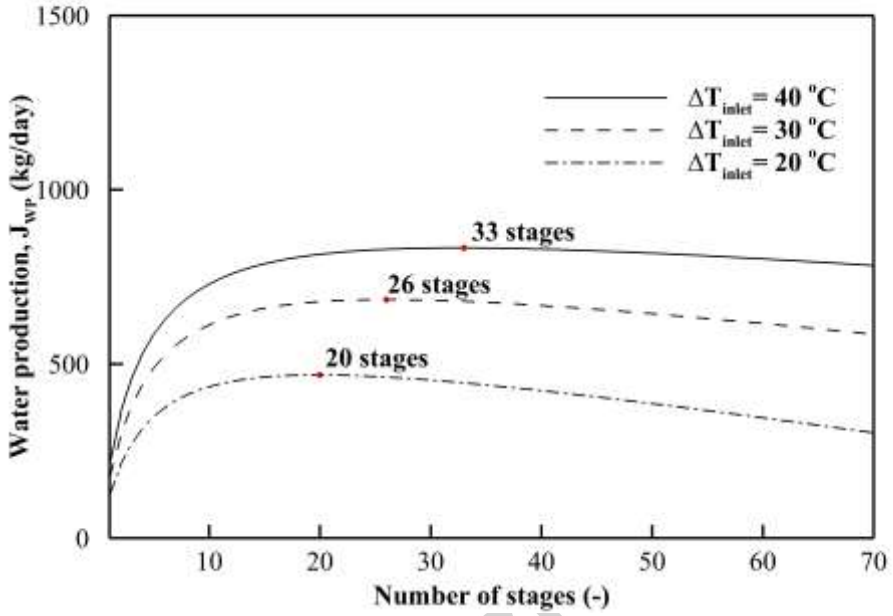

Figure 8. Effect of temperature difference from 40°C to 20°C on the mean permeate flux and water production at feed inlet temperature of 70°C and feed and permeate inlet flow rates of 10 L/min (case 2).

3.4 Influence of feed inlet temperature at constant feed and permeate inlet temperatures difference

The effect of feed inlet temperature on the WPI at constant inlet feed and permeate temperature difference (ΔT=20°C) was investigated at constant feed and permeate inlet flow rates (10 L/min). As shown in **Fig. 9**, the increase in feed inlet temperature caused the WPI to occur at lower number of DCMD stages. However, this effect is much lower than the effect of the inlet feed and permeate temperatures difference. Increasing the inlet feed temperature from 40°C to 80°C caused the WPI to occur at stage 19 instead of stage 25. The high inlet feed temperature leads the higher driving force represented by water vapor pressure difference as given by Eq. (7). Moreover, Figure 9 shows the increase of inlet feed

temperature causes WPI to occur at earlier stages. This demonstrates the significant contribution of mass transfer to heat transfer in the DCMD mode. This is due to the relatively high latent heat and high water vapor flux across the membrane generated by the higher inlet feed temperature causing an earlier convergence of lowest transmembrane temperature difference.

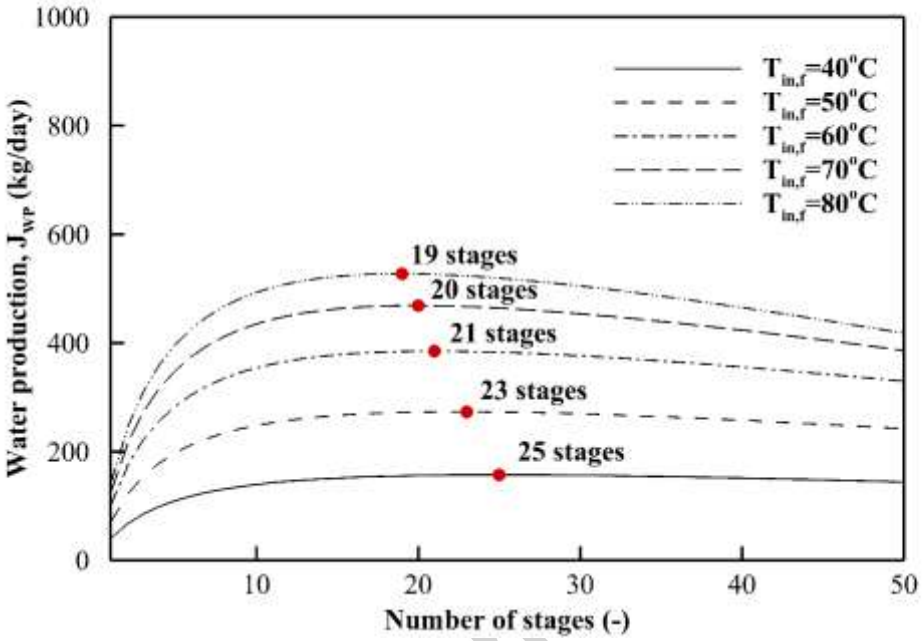

Figure 9. Effect of feed inlet temperature at constant temperature difference from 40°C to 80°C ((ΔT=20°C) on total water production, feed and permeate inlet flow rates = 10 L/min (case 3).

3.5 Influence of flow rate

Changing feed and permeate inlet flow rates has a significant effect on the performance of the MD process. Increasing feed and permeate inlet flow rates enhance the turbulence in the flow channel and near the membrane surface and improves the convection heat transfer coefficient. Consequently, it reduces temperature and concentration polarization effects on the water vapor flux [42]. **Fig. 10(a)** presents the effect of feed and permeate inlet flow rates ranging from 10 L/min to 25 L/min on the mean permeate flux. The mean permeate flux increases with an increase in the feed and permeate inlet flow rates. As shown in **Fig. 10(b)**, increasing the inlet feed and permeate flow rates delay the WPI and cause it to happen at higher number of DCMD stages. As a general rule, doubling the feed and permeate inlet flow

rates reduce the residence time inside the DCMD modules, which requires to double the number of stages in order for the WPI to occur. The increase of flow rate can increase the convection heat transfer at fixed operating conditions and module design. The convection heat transfer in the channel can improve both of temperature polarization and concentration polarization. Consequently, it increases the transmembrane temperature and delays to a later stage its convergence to its lowest value. In this study, the concentration polarization is not considered due to low local permeate flux. As shown in Fig. 10(a) and Fig. 10(b), the increased flow rate increases local permeate flux thus water production.

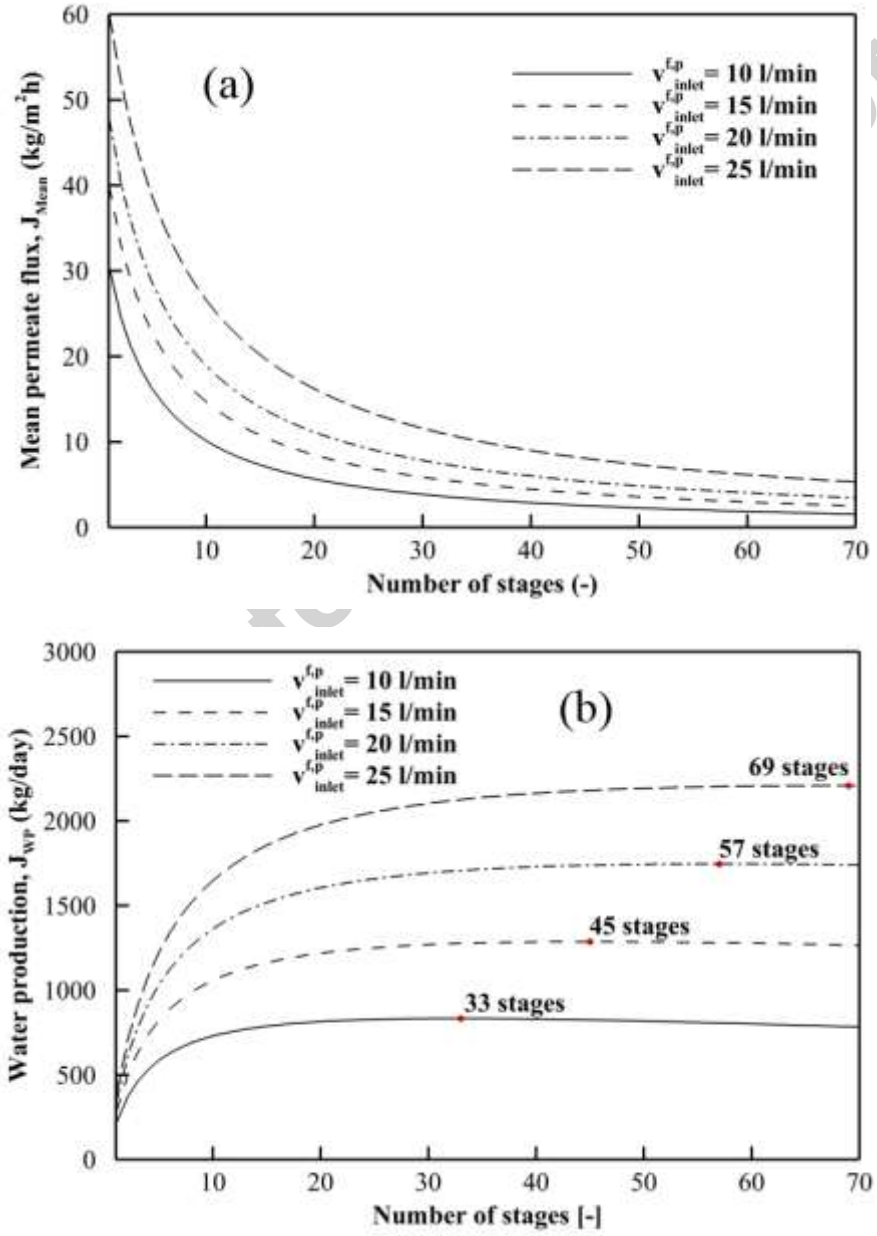

Figure 10. Effect of feed and permeate inlet flow rates from 10 L/min to 25 L/min on (a) the mean permeate flux, and (b) total water production at feed and permeate inlet temperatures of 70°C and 30°C, respectively (case 4).

3.6 Influence of feed salinity

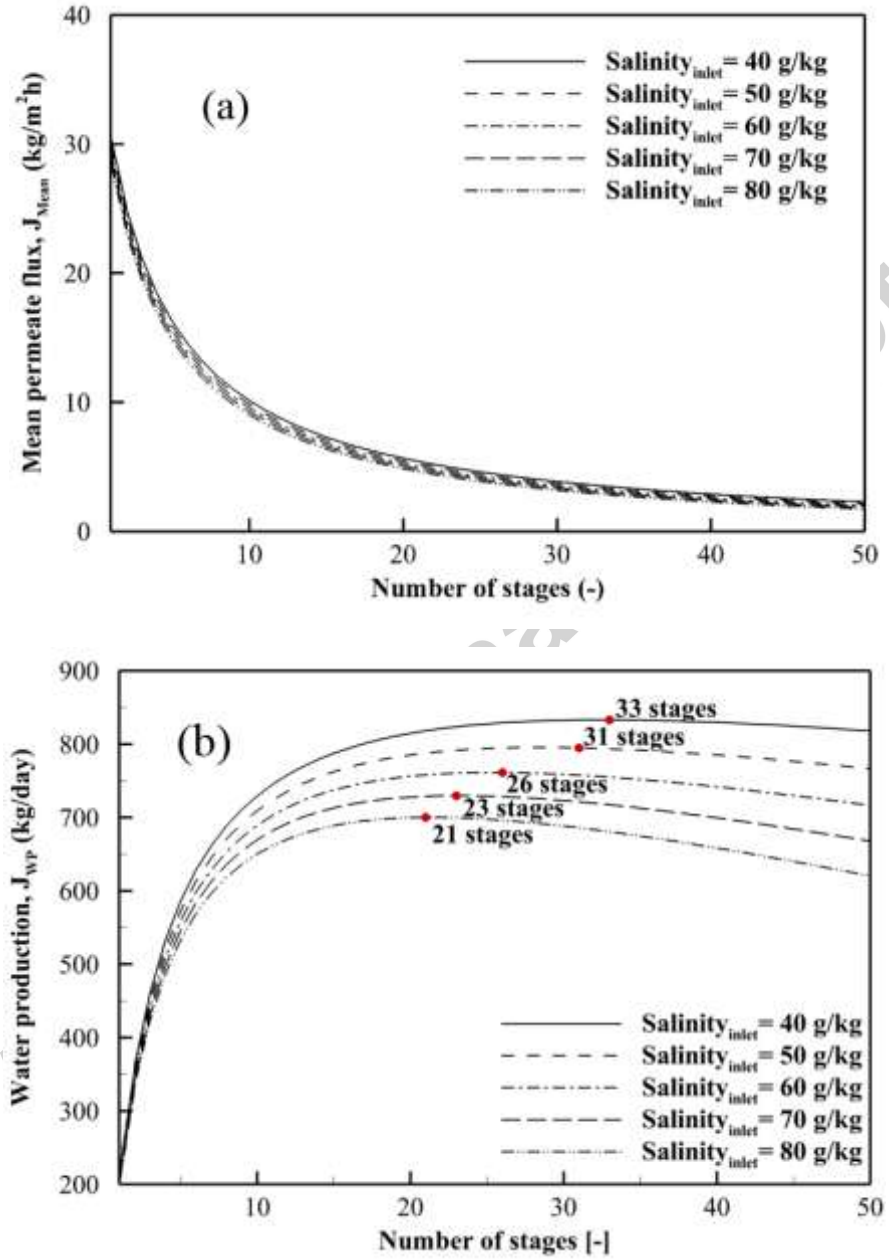

Figure 11. Effect of feed brine salinity from 40 g/kg to 80 g/kg on (a) the mean permeate flux, and (b) total water production at feed and permeate inlet temperatures of 70°C and 30°C, respectively, and feed and permeate inlet flow rates of 10 L/min (case 5).

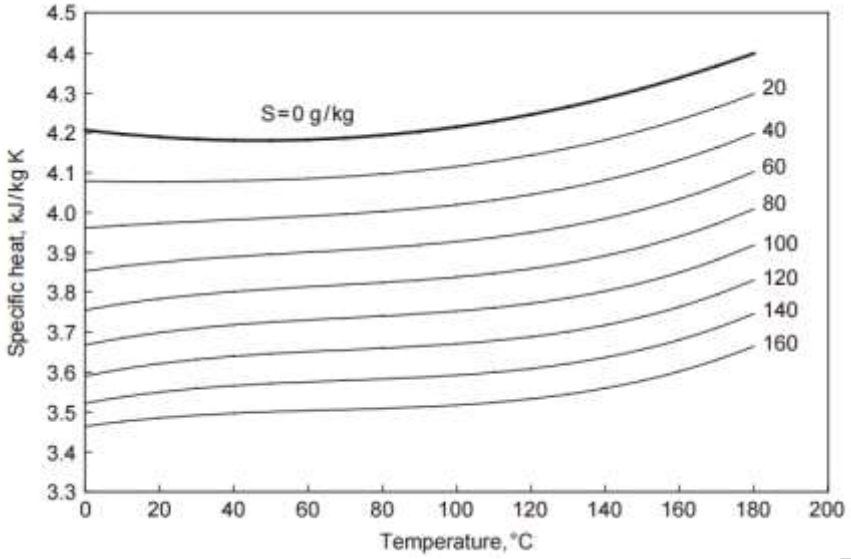

Figure 12. Effect of feed brine salinity from 0 g/kg to 160 g/kg on specific heat (kJ/kg K) with respect to temperatures from 0°C and 180°C [37]

The effect of the feed salinity was numerically investigated by varying the inlet concentrations ranging from 40 g/kg to 80 g/kg, which correspond to the Red Sea water salinity up to RO brine concentration [39]. Many researchers have reported the decrement of permeate flux with respect to the increment of brine salinity [43-47]. Our simulation results are in accordance with these reports, as shown in **Fig. 11(a)**. On the other hand, **Fig. 11(b)** shows that the feed inlet salinity has a moderate effect on WPI. Increasing feed salinity from 40 g/kg to 80 g/kg can cause the WPI to take place at earlier stage (at stage 21 instead of stage 33). The salinity of feed solution affects the properties of feed solution such as density, specific heat, viscosity, molar volume, and partial vapor pressure. Among all these properties, specific heat exhibits the most sensitive behavior, as shown in **Fig. 12**. Interestingly, the specific heat profile does not show a significant change with respect to temperature in the range from 40 °C to 80 °C, however it shows a major decrease when salinity changes. Due to the decrease of its specific heat, feed can easily lose thermal energy as the number of stages (or module length at constant membrane width) increases. The feed temperature of higher salinity feed solution can decrease more to produce water vapor across the membrane compared to the lower salinity feed solution according to the module length. And the low feed temperature of higher salinity decreased by the evaporation according to the module length also can lead to the lower partial pressure difference as driving force. Equivalently, a

low salinity feed solution which has higher specific heat can transport a higher thermal energy in the feed solution. Therefore, the increase in salinity decreases the heat energy of the feed, leading to an early convergence of the transmembrane temperature difference. Results suggest that salinity of inlet feed solution is an important process design parameter as it can also act upon WPI. As shown in **Fig. 11,** although the mean permeate flux profiles show a very small deviation according to the inlet feed salinity, the deviation of water production is not really small or negligible at large scale.

4. Conclusions

In this study, a theoretical investigation of a multi-stage DCMD process in cascade stack configuration has been conducted to investigate the WPI occurrence at various operating conditions. WPI phenomena can occur as a result of non-proper operating conditions, or module and system design. WPI may seem to occur at an unrealistic number of stages, although there is currently no information in the literature regarding specific size of future MD commercial plants. However, this research effort unveils a so far hidden phenomenon that we think is worth sharing with the scientific community, particularly process equipment designers, even if at this stage the WPI may seem unattainable. Simulations were performed for different values of the difference between feed and permeate inlet temperatures ranging from 30°C to 50°C while keeping a constant feed inlet temperature of 70°C. Another set of calculations was carried out by varying the feed and permeate volume flow rates from 10 L/min to 25 L/min as well as feed salinity from 40 g/kg to 80 g/kg. The WPI was observed in multi-stage DCMD process under given operating conditions due to the decrease in average water vapor flux and the increase in conductive heat loss as the membrane module length (at constant membrane width) increases. WPI is found to take place at lower membrane module length with a decreasing feed and permeate inlet temperatures difference, or feed and permeate inlet flow rates and increasing inlet feed temperature at constant feed to permeate temperature difference, or inlet feed salinity. Although the feed salinity has a negligibly negative effect on the mean permeate flux, it was clearly shown that it can affect WPI. Proper module scale-up is intimately linked to total production and MD plant size. Given a target production, module size and stacking can be carried out within the limits set by membrane properties and WPI risk of occurrence. The numerical methodology presented in this article can then be used to optimize feed and permeate inlet temperatures to set the

operating conditions at the maximum production rate.

Acknowledgements

The research reported in this paper was supported by King Abdullah University of Science and Technology (KAUST), Saudi Arabia. The authors acknowledge help, assistance and support from the Water Desalination and Reuse Center (WDRC) staff.

Nomenclature

A	Effective membrane area [m^2]
c_p	Specific heat capacity [kJ/kgK]
δ_m	membrane thickness [m]
h_c	Channel height [m]
ΔH_v	Enthalpy of evaporation at the mean temperature through the membrane
J_m	Mean permeate flux [kg/m^2h]
k	Conduction heat transfer coefficient [W/m^2K]
$\dot{m}_{f,in}$	Inlet feed mass flow rate [kg/hr]
S	Feed salinity [g/kg]
T	Temperature [K]
THE_{DCMD}	Total heat exchanged inside DCMD module [W/hr]
THE_{HX}	Total heat exchanged inside heat exchanged [W/hr]
$T_{f,in}$	Inlet feed temperature [K]
$T_{f,out}$	Outlet feed temperature [K]
$T_{p,in}$	Inlet permeate temperature [K]
v	Flow rates [L/min]
WPI	Water Production Inversion

Reference

[1] J.-G. Lee, Y.-D. Kim, W.-S. Kim, L. Francis, G. Amy, N. Ghaffour, Performance modeling of direct contact membrane distillation (DCMD) seawater desalination process using a commercial composite membrane, J. Membr. Sci., 478 (2015) 85-95.
[2] J.-G. Lee, Y.-D. Kim, S.-M. Shim, B.-G. Im, W.-S. Kim, Numerical study of a hybrid multi-stage vacuum membrane distillation and pressure-retarded osmosis system, Desalination, 363 (2015) 82-91.
[3] J.-G. Lee, W.-S. Kim, Numerical study on multi-stage vacuum membrane distillation with

economic evaluation, Desalination, 339 (2014) 54-67.
[4] S. Shim, J. Lee, W. Kim, Performance simulation of a multi-VMD desalination process including the recycle flow, Desalination, 338 (2014) 39-48.
[5] J.-G. Lee, W.-S. Kim, Numerical modeling of the vacuum membrane distillation process, Desalination, 331 (2013) 46-55.
[6] A. Alkhudhiri, N. Darwish, N. Hilal, Membrane distillation: A comprehensive review, Desalination, 287 (2012) 2-18.
[7] E. Curcio, E. Drioli, Membrane distillation and related operations—a review, Separation and Purification Reviews, 34 (2005) 35-86.
[8] Y.-D. Kim, K. Thu, N. Ghaffour, K.C. Ng, Performance investigation of a solar-assisted direct contact membrane distillation system, J. Membr. Sci., 427 (2013) 345-364.
[9] S. Al-Obaidani, E. Curcio, F. Macedonio, G. Di Profio, H. Al-Hinai, E. Drioli, Potential of membrane distillation in seawater desalination: thermal efficiency, sensitivity study and cost estimation, J. Membr. Sci., 323 (2008) 85-98.
[10] M. El-Bourawi, Z. Ding, R. Ma, M. Khayet, A framework for better understanding membrane distillation separation process, J. Membr. Sci., 285 (2006) 4-29.
[11] L.-H. Cheng, Y.-H. Lin, J. Chen, Enhanced air gap membrane desalination by novel finned tubular membrane modules, J. Membr. Sci., 378 (2011) 398-406.
[12] L.-H. Cheng, P.-C. Wu, J. Chen, Modeling and optimization of hollow fiber DCMD module for desalination, J. Membr. Sci., 318 (2008) 154-166.
[13] H. Maab, A. Al Saadi, L. Francis, S. Livazovic, N. Ghafour, G.L. Amy, S.P. Nunes, Polyazole hollow fiber membranes for direct contact membrane distillation, Industrial & Engineering Chemistry Research, 52 (2013) 10425-10429.
[14] L. Francis, N. Ghaffour, A.S. Alsaadi, S.P. Nunes, G.L. Amy, PVDF hollow fiber and nanofiber membranes for fresh water reclamation using membrane distillation, Journal of Materials Science, 49 (2014) 2045-2053.
[15] L. Francis, N. Ghaffour, A.A. Alsaadi, G.L. Amy, Material gap membrane distillation: a new design for water vapor flux enhancement, J. Membr. Sci., 448 (2013) 240-247.
[16] A. Alsaadi, N. Ghaffour, J.-D. Li, S. Gray, L. Francis, H. Maab, G. Amy, Modeling of air-gap membrane distillation process: a theoretical and experimental study, J. Membr. Sci., 445 (2013) 53-65.
[17] T.Y. Cath, V.D. Adams, A.E. Childress, Experimental study of desalination using direct contact membrane distillation: a new approach to flux enhancement, J. Membr. Sci., 228 (2004) 5-16.
[18] B. Li, K.K. Sirkar, Novel membrane and device for direct contact membrane distillation-based desalination process, Industrial & engineering chemistry research, 43 (2004) 5300-5309.
[19] H.C. Duong, P. Cooper, B. Nelemans, T.Y. Cath, L.D. Nghiem, Optimising thermal efficiency of direct contact membrane distillation by brine recycling for small-scale seawater desalination, Desalination, 374 (2015) 1-9.
[20] M. Khayet, T. Matsuura, Membrane distillation: principles and applications, Elsevier, 2011.
[21] K.L. Hickenbottom, T.Y. Cath, Sustainable operation of membrane distillation for enhancement of mineral recovery from hypersaline solutions, J. Membr. Sci., 454 (2014) 426-435.
[22] J.-G. Lee, E.-J. Lee, S. Jeong, J. Guo, A.K. An, H. Guo, J. Kim, T. Leiknes, N. Ghaffour, Theoretical modeling and experimental validation of transport and separation properties of carbon nanotube electrospun membrane distillation, J. Membr. Sci., (2016).

[23] J.-G. Lee, W.-S. Kim, J.-S. Choi, N. Ghaffour, Y.-D. Kim, A novel multi-stage direct contact membrane distillation module: Design, experimental and theoretical approaches, Water Res., 107 (2016) 47-56.
[24] S. Lin, N.Y. Yip, M. Elimelech, Direct contact membrane distillation with heat recovery: Thermodynamic insights from module scale modeling, J. Membr. Sci., 453 (2014) 498-515.
[25] Z. Ding, L. Liu, M.S. El-Bourawi, R. Ma, Analysis of a solar-powered membrane distillation system, Desalination, 172 (2005) 27-40.
[26] H.C. Duong, A.R. Chivas, B. Nelemans, M. Duke, S. Gray, T.Y. Cath, L.D. Nghiem, Treatment of RO brine from CSG produced water by spiral-wound air gap membrane distillation — A pilot study, Desalination, 366 (2015) 121-129.
[27] J. Blanco Gálvez, L. García-Rodríguez, I. Martín-Mateos, Seawater desalination by an innovative solar-powered membrane distillation system: the MEDESOL project, Desalination, 246 (2009) 567-576.
[28] C. Koroneos, G. Roumbas, Geothermal waters heat integration for the desalination of sea water, Desalination and Water Treatment, 37 (2012) 69-76.
[29] R. González-Bravo, F. Nápoles-Rivera, J.M. Ponce-Ortega, M. Nyapathi, N. Elsayed, M.M. El-Halwagi, Synthesis of optimal thermal membrane distillation networks, AlChE J., 61 (2015) 448-463.
[30] J.R. Welty, C.E. Wicks, G. Rorrer, R.E. Wilson, Fundamentals of momentum, heat, and mass transfer, John Wiley & Sons, 2009.
[31] E. Guillén-Burrieza, J. Blanco, G. Zaragoza, D.-C. Alarcón, P. Palenzuela, M. Ibarra, W. Gernjak, Experimental analysis of an air gap membrane distillation solar desalination pilot system, J. Membr. Sci., 379 (2011) 386-396.
[32] Y.-D. Kim, K. Thu, S.-H. Choi, Solar-assisted multi-stage vacuum membrane distillation system with heat recovery unit, Desalination, 367 (2015) 161-171.
[33] P.A. Hogan, Sudjito, A.G. Fane, G.L. Morrison, Proceedings of the Twelfth International Symposium on Desalination and Water Re-useDesalination by solar heated membrane distillation, Desalination, 81 (1991) 81-90.
[34] M.S. El-Bourawi, Z. Ding, R. Ma, M. Khayet, A framework for better understanding membrane distillation separation process, J. Membr. Sci., 285 (2006) 4-29.
[35] A.M. Karam, T.M. Laleg-Kirati, Electrical equivalent thermal network for direct contact membrane distillation modeling and analysis, Journal of Process Control, 47 (2016) 87-97.
[36] A.M. Karam, A.S. Alsaadi, N. Ghaffour, T.M. Laleg-Kirati, Analysis of direct contact membrane distillation based on a lumped-parameter dynamic predictive model, Desalination, 402 (2017) 50-61.
[37] M.H. Sharqawy, J.H. Lienhard, S.M. Zubair, Thermophysical properties of seawater: a review of existing correlations and data, Desalination and Water Treatment, 16 (2010) 354-380.
[38] S. Al-Sharif, M. Albeirutty, A. Cipollina, G. Micale, Modelling flow and heat transfer in spacer-filled membrane distillation channels using open source CFD code, Desalination, 311 (2013) 103-112.
[39] J. Phattaranawik, R. Jiraratananon, A. Fane, Effects of net-type spacers on heat and mass transfer in direct contact membrane distillation and comparison with ultrafiltration studies, J. Membr. Sci., 217 (2003) 193-206.
[40] J. Phattaranawik, R. Jiraratananon, A. Fane, C. Halim, Mass flux enhancement using spacer filled channels in direct contact membrane distillation, J. Membr. Sci., 187 (2001) 193-201.
[41] A. Da Costa, A. Fane, D. Wiley, Spacer characterization and pressure drop modelling in

spacer-filled channels for ultrafiltration, J. Membr. Sci., 87 (1994) 79-98.
[42] A.S. Alsaadi, L. Francis, G.L. Amy, N. Ghaffour, Experimental and theoretical analyses of temperature polarization effect in vacuum membrane distillation, J. Membr. Sci., 471 (2014) 138-148.
[43] C.R. Martinetti, A.E. Childress, T.Y. Cath, High recovery of concentrated RO brines using forward osmosis and membrane distillation, J. Membr. Sci., 331 (2009) 31-39.
[44] Y. Yun, R. Ma, W. Zhang, A.G. Fane, J. Li, Direct contact membrane distillation mechanism for high concentration NaCl solutions, Desalination, 188 (2006) 251-262.
[45] D. Winter, J. Koschikowski, M. Wieghaus, Desalination using membrane distillation: Experimental studies on full scale spiral wound modules, J. Membr. Sci., 375 (2011) 104-112.
[46] A. Alkhudhiri, N. Darwish, N. Hilal, Treatment of high salinity solutions: Application of air gap membrane distillation, Desalination, 287 (2012) 55-60.
[47] J. Xu, Y.B. Singh, G.L. Amy, N. Ghaffour, Effect of operating parameters and membrane characteristics on air gap membrane distillation performance for the treatment of highly saline water, J. Membr. Sci., 512 (2016) 73-82.

Highlights

- Water production inversion (WPI) is observed in multi-stage DCMD.
- It is due to average flux drop and conduction losses increase for longer modules.
- WPI was confirmed using two different mathematical models validated experimentally.
- Optimum number of stages has been set for various operating conditions.
- Feed salinity has a significant influence on WPI.